Journal of Control, Automation and Electrical Systems (2020) 31:1210–1220
https://doi.org/10.1007/s40313-020-00617-5

Robust Observer-Based Sliding Mode Control for Maximum Power Point Tracking

Amruta S. Deshpande[1] · **S. L. Patil**[1]

Received: 17 July 2019 / Revised: 16 March 2020 / Accepted: 3 June 2020 / Published online: 18 June 2020

Abstract
This paper presents a new observer-based maximum power point tracking technique (MPPT) for the solar panel system. Apart from fulfilling the main objective of MPPT, it is designed to accomplish the task without having the measure solar panel output voltage and with a chatter-free control. The proposed control strategy employs a disturbance observer to do away with the need to sense solar panel output voltage and also to ensure insensitivity of uncertainties. A special state observer enables operating the system even when the converter output voltage is initially zero. The performance of the algorithm is assessed for robustness towards the parasitics and uncertainties. The scheme is validated by simulation as well as experimentation in the laboratory.

Keywords Photovoltaic cell · Maximum power point tracking · Sliding mode control · Disturbance observer

1 Introduction

The optimum utilization of sustainable energy helps to reduce the global level energy crisis. The solar energy is one of the clean energies and spreads across the world free of cost. The drawback of the solar panel is the very low conversion efficiency, as it depends on several factors such as irradiance, environmental temperature, dirt, loading condition and solar panel type. The improvement in the efficiency of the solar panel is possible at the manufacturing stage and conversion stage. In the conversion stage, the suitable converter topology helps to improve the efficiency with maximum power point tracking (MPPT) algorithm. These algorithms help to extract maximum energy from the solar panel in the presence of changing environmental conditions. The various types of dc–dc converter optimize the match between the solar panel and load. The boost converter is one of the preferred converters in photovoltaic (PV) application because of its higher efficiency and operation under continuous conduction mode helps to extract maximum energy from the solar cell (Glasner and Appelbaum 1996).

In the MPPT literature, algorithms, viz. perturb and observe (P&O) (Femia et al. 2005) and incremental conductance (IC) (Lin et al. 2011), are popular on account of the simplicity of their architecture and ease of implementation. The main drawbacks of the P&O and IC algorithms are continued oscillations and requirement of sensors for current and voltage. The drawbacks can be removed by improving the existing algorithm (Yong and Huiqing 2019; Abdel-Salam et al. 2018; Rezaei 2019). The algorithms like ripple correlation control (RCC) (Esram et al. 2006) and extremum seeking control (ESC) (Heydari-doostabad et al. 2013) are well suited for low-cost application, but these algorithms too suffer from oscillation in the output. These algorithms require sensors for current and voltage measurement. Soft computing-based algorithms, which include fuzzy logic (Alajmi et al. 2011) and fuzzy proportional derivative (Moçambique et al. 2015) and neural network (Veerachary et al. 2003), have attracted many researchers due to their flexibility and robustness. However, accurate and large data requirement is the drawback associated with these algorithms. A comparative study of all these methods is useful to select a suitable algorithm to obtain power maxima (Subudhi and Pradhan 2013; Salas et al. 2006).

The nature of (current–voltage) IV and (power–voltage) PV characteristics of solar cells is nonlinear, and therefore,

✉ Amruta S. Deshpande
asd.instru@coep.ac.in

S. L. Patil
slp.instru@coep.ac.in

[1] Department of Instrumentation and Control, College of Engineering Pune, Pune, India

the nonlinear controller will be an appropriate choice for the PV system. Sliding mode control (SMC) is one of the promising techniques because of its various features like parameter variation insensitivity, robust nature and good performance under disturbance rejection (Utkin 1993). Conventional SMC implemented on the solar PV system (Chu et al. 2009) uses a ratio of change in power to change the converter current as a sliding surface. The algorithm requires measurement of output voltage and current of solar panel as well as the output voltage of the converter. The modified SMC considers the effect of disturbances and tracks maximum solar power (Mojallizadeh et al. 2016). The control employs a signum function which results in output chatter. In addition, the implementation of the control needs sensors for the measurement of output voltage and output current of the solar panel and output voltage of the converter. Finite-time SMC can be effectively applied to the grid connected photovoltaic array (Dhar and Dash 2015), but in this method too current and voltage sensors are required for the implementation.

In sliding mode control implementation, chattering resulting from discontinuous control is a major problem. The combination of a disturbance observer (DO) with SMC can do away with the need for a discontinuous control and remove the problem of chatter. Interestingly, as shown in this paper, the DO can make it possible to reduce the sensor requirement. The various methods for uncertainty estimate including disturbance observer (DO) (Chen 2004; Chen et al. 2016) are discussed in the literature. There is a diversity of applications investigated such as flexible joint manipulator system (Ginoya et al. 2014), ball and beam system (Zhang et al. 2016), fractional-order Chua's system (Chen et al. 2017) for DO. The parametric uncertainty can be estimated for the PV application to improve the performance of the tracking controller (Sitbon et al. 2015). Second-order terminal sliding mode control is used for maximum power extraction with finite-time convergence (Abolvafaei and Ganjefar 2019).

From the existing literature, it is seen that most of the reported results require three sensors. It would be desirable to reduce this requirement. An improvement in the SMC approach is required to avoid the chattering associated with it. Further, the current SMC approaches do not work satisfactorily if the initial condition for output voltage is zero. This paper attempts to overcome the above drawbacks by proposing a new kind of observer combined with DO. The main features of the present paper are:

1. New observer-based SMC where the initial condition of output voltage V_o can be zero.
2. The need for a sensor to measure V_p is avoided.
3. Robustness to uncertainties in solar irradiation, temperature and output load without knowledge of even the bounds of these uncertainties.
4. Robustness to parasitics without any change in control law.
5. Validation by simulation and experimentation.

The paper is organized as follows: Section 1 presents introduction. Section 2 describes the PV system. Section 3 presents controller design, and Sect. 4 describes the stability of the proposed algorithm. Sections 5 and 7 include simulation and hardware results.

2 System Description and Problem Formulation

The objective of the control design is to track maximum power in presence of varying environmental conditions. The block diagram of the PV system in given in Fig. 1.

PV system composed of hardware components like PV array, dc–dc boost converter and MPPT controller. The parameters of the PV array, dc–dc boost converter and MPPT controller are given in Table 1. All parameters except control are taken from the literature Mojallizadeh et al. (2016).

2.1 PV Array

The PV array is formed by the series and parallel combination of various PV module. The single-diode module is composed of the light source, diode, series resistance and parallel resistance (Chu et al. 2009). The output current I_p of the PV cell is given by

$$I_\mathrm{p} = N_\mathrm{p} I_\mathrm{ph} - N_\mathrm{p} I_\mathrm{rs}\left[\exp\left(\frac{q V_\mathrm{p}}{N_\mathrm{s} A k_\mathrm{o} T}\right) - 1\right] \tag{1}$$

$$I_\mathrm{ph} = I_\mathrm{s} + K_i[T - T_\mathrm{ref}]\frac{G}{1000} \tag{2}$$

$$I_\mathrm{rs} = I_r\left(\frac{T}{T_\mathrm{ref}}\right)^3\left[\exp\left(\frac{q.E_\mathrm{go}}{k_\mathrm{o} A}\right)\left(\frac{1}{T_\mathrm{ref}} - \frac{1}{T}\right)\right] \tag{3}$$

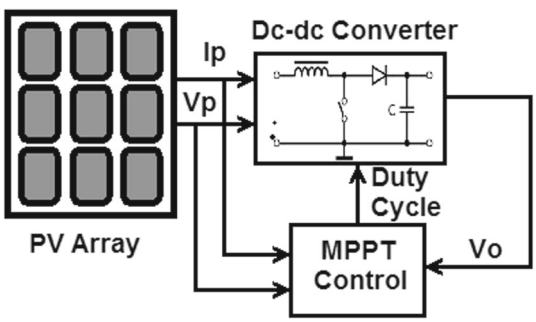

Fig. 1 PV system

Table 1 Nomenclature

Parameter	Description
V_p, I_p	Solar array output voltage (V), output current (A)
V_o, I_o	Converter output voltage (V), converter current (A)
I_{ph}	Generated photocurrent (A)
I_{rs}	Reverse saturation current at standard condition (A)
I_s	Short-circuit current at standard condition (3.81 A)
I_r	Reverse saturation current of solar cell (5.981×10^{-8} A)
K_i	Short-circuit temperature coefficient (0.0024 A/K)
k_o	Boltzmann constant (1.38×10^{-23} J/K)
T_{ref}	Reference temperature (298 K)
T	PV module temperature (K)
q	Electron charge (1.60217×10^{-19} C)
G	Solar irradiance (W/m^2)
A	Diode ideality factor (1.2)
R_s, R_p	Series, parallel resistance of a cell
N_p, N_s	Solar array number of parallel, series cells
E_{go}	Band gap energy (1.12)
L	Inductor (1.5 mH)
C	Capacitor (470 μF)
R	Load resistance (100 Ω)
P_1, P_2	Auxiliary variables
M_1, M_2	User-chosen observer gain
K, K_1, K_2	User-chosen constants
d_1, d_2	User-chosen constants

where I_{ph} is the photo current and I_{rs} is the reverse saturation current at standard condition. The series and parallel combination of PV cell constitutes a PV array. The output of PV array is given to dc–dc boost converter.

2.2 Dc–dc Boost Converter

The MPPT controller generates duty cycle in order to create switching signals in the form of pulse width modulation(PWM) signal. The state equations of boost converter are given by

$$\dot{x}_1 = \frac{-(1-u)}{L}x_2 + \frac{V_p}{L} \tag{4}$$

$$\dot{x}_2 = \frac{(1-u)}{C}x_1 - \frac{1}{RC}x_2 \tag{5}$$

where x_1 is solar panel output current (I_p) and x_2 is converter output voltage (V_o). R, L and C are the parameters of converter, and u is the duty ratio. From (4) and (5), it is clear that for implementing conventional sliding mode control minimum three sensors are required (x_1, x_2 and V_p). It can be noted from (4) that the expression for control u would involve x_2 in the denominator. This makes the control to be undefined if $x_2 = 0$ at $t = 0$. If the initial condition of x_2 is zero, the control effort will be infinite. This suggests the need for a special controller.

3 Design of Control

The problem mentioned in Sect. 2 can be overcome by

(a) Proposing a DO to estimate the uncertainties in (4) and (5)
(b) Proposing a state observer to estimate the states x_1 and x_2.
(c) Proposing a sliding surface based on the estimated states.

In this section, the controller is developed step by step to overcome the above mentioned problem. The design of a DO is considered next.

3.1 Design of DO

First, the boost converter Eqs. (4) and (5) are re-framed as

$$\dot{x}_1 = \frac{-(1-u)}{L}x_2 + \frac{d_1}{L} \tag{6}$$

$$\dot{x}_2 = \frac{(1-u)}{C}x_1 + \frac{d_2}{C} \tag{7}$$

where $d_1 = V_p$ and $d_2 = \frac{-x_2}{R}$. Notice that V_p for which several previously reported schemes needed a sensor is now part of the disturbance d_1 and the unknown load R is now part of the disturbance d_2. If d_1 can be estimated using a DO, then the need to sense V_p is removed, and if d_2 can be estimated, that gives robustness to unknown load.

$$\hat{d}_1 = P_1 + M_1 x_1 \tag{8}$$

where $\hat{d}_1$ is an estimation of d_1, P_1 is an auxiliary variable and $M_1 > 0$ is an user-chosen observer gain.

$$\dot{P}_1 = -M_1\left[\frac{-(1-u)x_2}{L} + \frac{\hat{d}_1}{L}\right] \tag{9}$$

Taking derivative of (8) and using (9), we obtain

$$\dot{\hat{d}}_1 = -M_1\left[\frac{-(1-u)x_2}{L} + \frac{\hat{d}_1}{L}\right] + M_1\left[\frac{-(1-u)x_2}{L} + \frac{d_1}{L}\right] \tag{10}$$

$$\dot{\hat{d}}_1 = \frac{M_1}{L}(d_1 - \hat{d}_1) \tag{11}$$

The disturbance estimation error $\tilde{d}_1$ is defined as

$$\tilde{d}_1 = d_1 - \hat{d}_1 \tag{12}$$

Subtracting $\dot{d}_1$ from both sides of (11)and using (12), we obtain

$$\dot{\tilde{d}}_1 = \dot{d}_1 - \frac{M_1}{L}\tilde{d}_1 \tag{13}$$

On similar lines, disturbance d_2 can be estimated using DO

$$\hat{d}_2 = P_2 + M_2 x_2 \tag{14}$$

where $\hat{d}_2$ is an estimation of d_2, P_2 is an auxiliary variable and $M_2 > 0$ is an user-chosen observer gain.

$$\dot{\tilde{d}}_2 = \dot{d}_2 - \frac{M_2}{C}\tilde{d}_2 \tag{15}$$

The boundedness of the disturbance estimation error is proved in Sect. 4.

3.2 Design of State Observer

In this section, a state observer is designed to estimate the states x_1 and x_2. On the face of it, it looks strange to design a state observer when in fact the states are available but the motivation for such an observer will become clear later. Consider the observer given by

$$\dot{\hat{x}}_1 = \frac{-(1-u)}{L}\hat{x}_2 + \frac{\hat{d}_1}{L} + K_1(x_1 - \hat{x}_1) \tag{16}$$

$$\dot{\hat{x}}_2 = \frac{(1-u)}{C}\hat{x}_1 + \frac{\hat{d}_2}{C} + K_2(x_2 - \hat{x}_2) \tag{17}$$

where $K_1 > 0$ and $K_2 > 0$ user-chosen are constants. Define the estimation error as $\tilde{x} = [\tilde{x}_1\ \tilde{x}_2]^T$ with $\tilde{x}_1 = x_1 - \hat{x}_1$ and $\tilde{x}_2 = x_2 - \hat{x}_2$. Now subtracting (16), (17) from (4) and (5), respectively, we obtain

$$\dot{\tilde{x}}_1 = \frac{-(1-u)}{L}\tilde{x}_2 + \frac{\tilde{d}_1}{L} - K_1(\tilde{x}_1) \tag{18}$$

$$\dot{\tilde{x}}_2 = \frac{(1-u)}{C}\tilde{x}_1 + \frac{\tilde{d}_2}{C} - K_1(\tilde{x}_2) \tag{19}$$

The stability of the observer is defined in Sect. 4.

3.3 Observer-Based SMC

It is known that if $I_p = x_1$ can be forced to a reference current $I_{\text{ref}} = 0.85 I_{\text{p}}$ Alghuwainem (1994), then MPPT is assured. Therefore, a sliding surface

$$\sigma = x_1 - I_{\text{ref}} \tag{20}$$

Table 2 Control parameter

Mojallizadeh		Proposed controller	
Parameter	Value	Parameter	Value
k	0.001	K	0.2
δ	0.01	K_1, K_2	400
η_0	0.1	M_1, M_2	20

is a natural choice for a sliding surface. If a control is designed using (20), it can be seen that the control is not defined at $t = 0$, if the output voltage x_2 is 0 at start. Therefore, consider a new sliding surface given by

$$\hat{\sigma} = \hat{x}_1 - I_{\text{ref}} \tag{21}$$

Differentiating (21) and using (16), we obtain

$$\dot{\hat{\sigma}} = -(1-u)\frac{\hat{x}_2}{L} + \frac{\hat{d}_1}{L} + K_1(x_1 - \hat{x}_1) \tag{22}$$

We select the control

$$u = u_1 + u_2 \tag{23}$$

where

$$u_1 = 1 - \frac{KL\hat{\sigma}}{\hat{x}_2} \tag{24}$$

$$u_2 = -\frac{\hat{d}_1}{\hat{x}_2} - \frac{K_1 L \tilde{x}_1}{\hat{x}_2} \tag{25}$$

resulting in

$$\dot{\hat{\sigma}} = -K\hat{\sigma} \tag{26}$$

where $K > 0$ is a user-chosen constant, notice that

$$u = 1 - \frac{L}{\hat{x}_2}\left(\frac{\hat{d}_1}{L} + K_1\tilde{x}_1 + K\hat{\sigma}\right) \tag{27}$$

In this case, u will not be unbounded at t=0, even if $x_2(0) = 0$ because x_2 does not appear in (27). The initial value of $\hat{x}_2$ appearing in (27) can always be chosen by the designer overcoming the problem completely. The values of the constants are given in Table 2.

4 Stability

The stability of system can be analyzed by finding the dynamics of $\tilde{d}_1, \tilde{d}_2, \tilde{x_1}$ and $\tilde{x_2}$. The stability is based on the concept

of ultimate boundedness. For finding the bounds for d_1 and d_2 Lyapunov's criteria are used.

$$V_1(\tilde{d}_1) = \frac{1}{2}\tilde{d}_1^2 \tag{28}$$

Differentiating (28) and using (13), we obtain

$$\begin{aligned}\dot{V}_1(\tilde{d}_1) &= \tilde{d}_1\left(\dot{d}_1 - \frac{M_1}{L}\tilde{d}_1\right)\\ &\leq -\frac{M_1}{L}\tilde{d}_1^2 + |\tilde{d}_1\dot{d}_1|\\ &\leq -|\tilde{d}_1|\left[\frac{M_1}{L}|\tilde{d}_1| - |\dot{d}_1|\right]\end{aligned} \tag{29}$$

with assumption on $|\dot{d}_1| \leq \mu_1$. From (29), using the notion of ultimate boundedness (Corless and Leitmann 1981), it can be proved that the estimation error $|\tilde{d}_1|$ is ultimately bounded and the bound is given by

$$|\tilde{d}_1| \leq \lambda_1 \tag{30}$$

where λ_1 is given by

$$\lambda_1 = \frac{L\mu_1}{M_1} \tag{31}$$

Since V_p is constant for given scenario, the value of $\dot{d}_1$ is zero and hence the value of $\mu_1 = 0$. In this scheme, a stronger result is obtained which gives asymptotic stability for $\tilde{d}_1$, i.e.,

$$|\tilde{d}_1| \to 0 \tag{32}$$

On similar line, bounds for d_2 can be determined as

$$\begin{aligned}\dot{V}_2(\tilde{d}_2) &= \tilde{d}_2\left(\dot{d}_2 - \frac{M_2}{C}\tilde{d}_2\right)\\ |\tilde{d}_2| &= |\dot{d}_2|\frac{C}{M_2} = \lambda_2\end{aligned} \tag{33}$$

$$\lambda_2 = \frac{C\mu_2}{M_2} \tag{34}$$

with the assumption on $|\dot{d}_2| \leq \mu_2$. Since of x_2 and R are constant for given scenario, the value of $\dot{d}_2$ is zero and hence the value of $\mu_2 = 0$. In this scheme, the result is obtained which gives asymptotic stability for $\tilde{d}_2$, i.e.,

$$|\tilde{d}_2| \to 0 \tag{35}$$

Bounds of $\tilde{d}_1$ can be lowered by increasing M_1, and bounds of $\tilde{d}_2$ can be lowered by increasing M_2. Consider a Lyapunov function given below.

$$V = \frac{1}{2}L\tilde{x}_1^2 + \frac{1}{2}C\tilde{x}_2^2 \tag{36}$$

Differentiating (36) and using (18), (19), (13) and (15), the stability of the $\tilde{x}_1$ and $\tilde{x}_2$ can be analyzed as follows.

$$\begin{aligned}\dot{V}(\hat{\sigma}) &= \tilde{x}_1\tilde{d}_1 - \tilde{x}_2\tilde{d}_2 - K_1\tilde{x}_1^2L - K_2\tilde{x}_2^2C\\ &\leq -K_1L\tilde{x}_1^2 + |x_1|\lambda_1 - K_2C\tilde{x}_2^2 + |x_2|\lambda_2\\ &\leq -|\tilde{x}_1|(K_1L|\tilde{x}_1| - \lambda_1) - |\tilde{x}_2|(K_2C|\tilde{x}_2| - \lambda_2)\end{aligned} \tag{37}$$

$$|\tilde{x}_1| = \frac{\lambda_1}{K_1L}, |\tilde{x}_2| = \frac{\lambda_2}{K_2C} \tag{38}$$

In view of the comments regarding the asymptotic stability of $\tilde{d}_1, \tilde{d}_2$, it follows that (38) will get modified as $|\tilde{x}_1| \to 0$ and $|\tilde{x}_2| \to 0$ as $t \to \infty$. The bound on $\tilde{x}_1$ and $\tilde{x}_2$ can be lowered by increasing K_1, K_2. Hence, the stability of the proposed observer-based control law is proved.

5 Simulation Results

The proposed control scheme is assessed by simulation for three scenarios and effectiveness of the scheme in terms of estimation accuracy and robustness to the parasitics. The scheme is compared with a recent result based on different sliding surface (Mojallizadeh et al. 2016). The standard reference conditions considered for irradiation is 1000 W/m^2, temperature is 25 °C, and load resistance is 100 Ω. Also the simulation is carried out to analyze the initial condition effect, accuracy of estimation and parasitics effect on proposed scheme.

5.1 Simulation Cases

A change in environmental parameters causes a change in the output power of the solar panel. Simulation is carried out to see the effect of variation of irradiation, temperature and load resistance and compared with the standard condition. The details of the four cases are given in Table 3. The results obtained with the proposed method are compared with Mojallizadeh et al. (2016) which employs a sliding surface as

$$s = 2R_\mathrm{p} + I_\mathrm{p}\frac{\partial R_\mathrm{p}}{\partial I_\mathrm{p}} \tag{39}$$

under a control signal u given by

$$u = u_{eq} + u_n \tag{40}$$

$$u_{eq} = 1 - \frac{V_p}{V_o} \tag{41}$$

Table 3 Simulation condition cases

Case no.	Parameter variation	G(W/m^2)	T(°C)	R(Ω)
1	Irradiation	550–1000	25	100
2	Temperature	1000	50–25	100
3	Resistance	1000	25	50–100

$$u_n = \eta_0(|s| + \delta).sgn(s) + k.s \tag{42}$$

The $R_p = V_p/I_p$. The values of the simulation parameters k, δ and η_0 are given in Table 2 and are considered from Mojallizadeh et al. (2016). From Eqs. (40) and (41), it is observed that the sensor is required for the measurement of solar panel output voltage V_p and consists of V_o parameter in the denominator of control signal, which states that very low initial condition of V_o requires very large control signal.

5.2 Case 1

Simulation is carried out for the changing condition of irradiation. The irradiation is varied from 550 to 1000 W/m^2. Figure 2 shows transient response of current and voltage for change in irradiation condition. The proposed algorithm is compared with conventional SMC (Mojallizadeh et al. 2016). Figure 2a shows the variation of irradiation input. Figure 2b, c shows the variation of the solar panel output current and voltage. Figure 2d, e shows the variation of converter output current and voltage variation for case 1.

Figure 2 shows that the response time of the proposed controller is faster than the conventional sliding mode control for a change in irradiation condition.

5.3 Case 2

Simulation is carried out for the changing temperature condition with irradiation and load resistance as constants. The temperature of the solar panel is varied from 50 to 25 °C. Figure 3a shows the variation of temperature input. Figure 3b, c shows the variation of the solar panel output current and voltage. Figure 3d, e shows the variation of converter output current and voltage variation for case 2. Figure 3 shows that the response time of the proposed controller is faster than the conventional sliding mode control for a change in temperature condition.

5.4 Case 3

Simulation is carried out for the changing load condition with irradiation and temperature as constants. The load is varied from 50 to 100 Ω. Figure 4a shows the variation of load condition. Figure 4b, c shows the variation of the solar panel output current and voltage. Figure 4d, e shows the variation

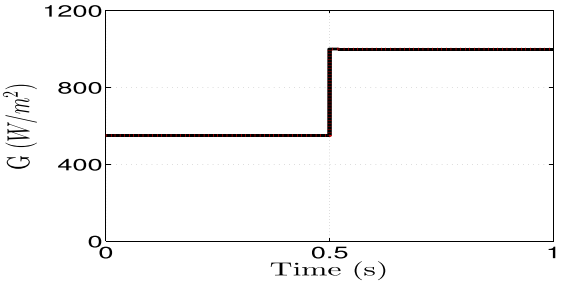

(a) Irradiation Variation

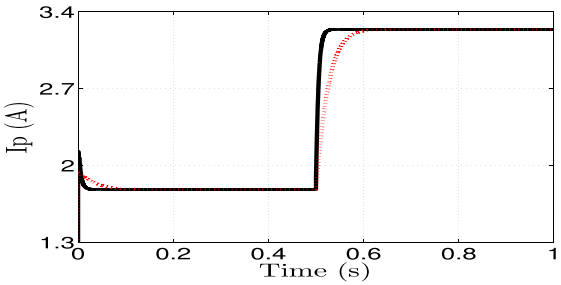

(b) Solar panel output current variation

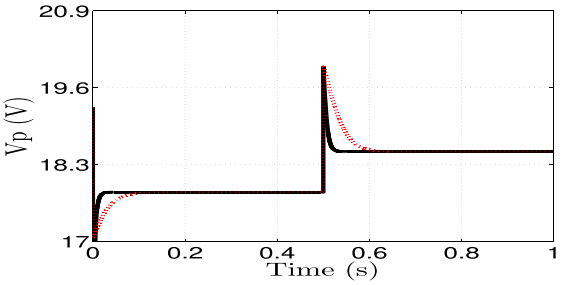

(c) Solar panel output voltage variation

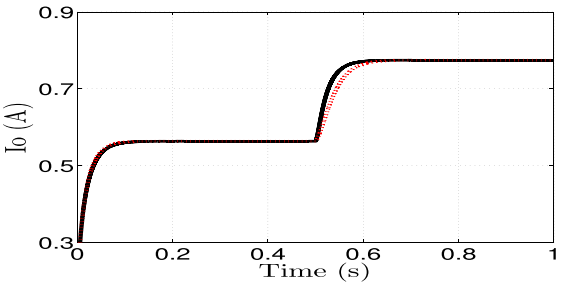

(d) Converter output current variation

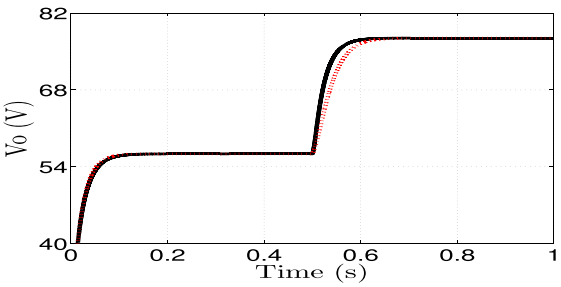

(e) Converter output voltage variation

Fig. 2 Comparison of the proposed method (black) with (Mojallizadeh et al. 2016) (dotted red) under varying irradiation condition (Case 1)

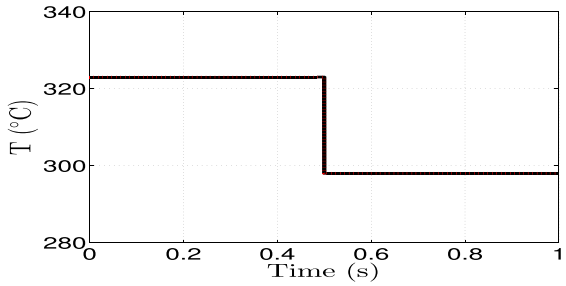

(b) Temperature Variation

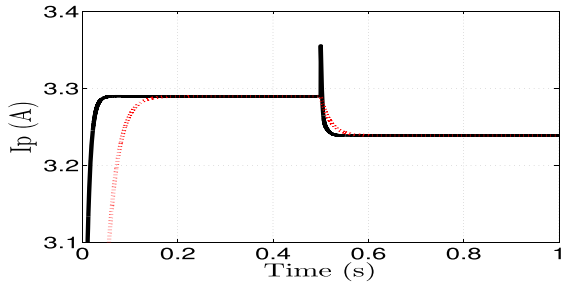

(b) Solar panel output current variation

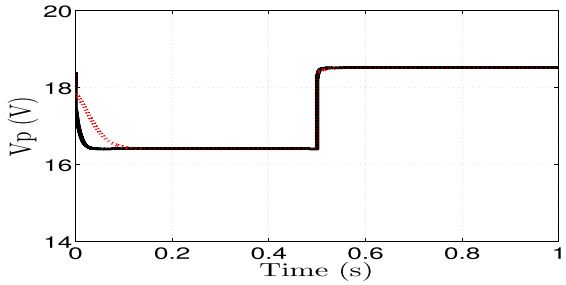

(c) Solar panel output voltage variation

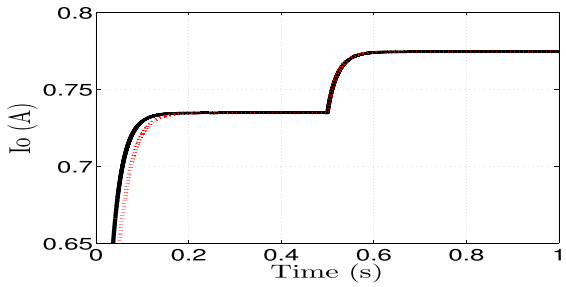

(d) Converter output current variation

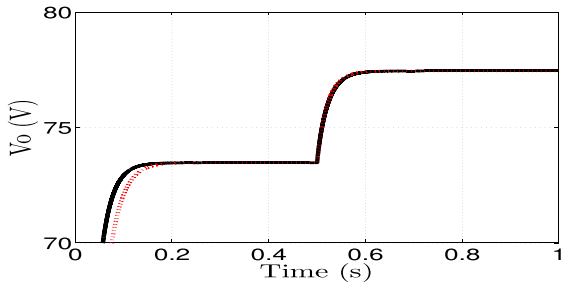

(e) Converter output voltage variation

Fig. 3 Comparison of the proposed method (black) with (Mojallizadeh et al. 2016) (dotted red) under varying temperature condition (Case 2)

of converter output current and voltage variation for case 2. Figure 4 shows that, in conventional control, estimate of the disturbance is not taken into consideration; hence, response time of the proposed controller is smaller than the conventional sliding mode control for a change in load condition. The MPPT algorithm extracts maximum power at given environmental condition and maintains the constant power in case of changing load condition.

5.5 Effect on the initial condition

The plot for x_2 with equivalent control is shown in Fig. 5a. The equivalent control considers the term $V_o = x_2$ in the denominator. If $V_o(0) = 0$, the value of the control is infinite. Here, the simulation is carried out with $V_o(0) = 0$ for Mojallizadeh et al. (2016) and for proposed controller as shown in Fig. 5a. The plot for $\hat{x}_2$ where $\hat{x}_2(0) \neq 0$ is shown in Fig. 5b. $\hat{x}_2$ is the estimated value of the output voltage x_2. From the plot, it is clear that even if the initial value of the control is zero for the proposed controller, the output x_2 gives satisfactory response.

5.6 Estimation accuracy

The design of observer facilitates the accuracy of an estimate d_1 and d_2 given by $d_1 = V_p$ and $d_2 = \frac{-x_2}{R}$. Figure 6a shows that estimate of input voltage d_1 is varied from 17 to 18 V at 0.35 s and 18–16 V at 0.55 s. As shown in (32), if d_1 is constant, the estimation error is zero at steady state. Similarly, in Fig. 6b the estimate d_2 is varied from -1.1 to -0.775V/Ω at 0.5 s. The change in the estimation d_2 is carried out using a subsequent change in load resistance value. As d_2 is constant, the estimation error is zero at steady-state condition. On similar line, estimation accuracy is plotted for $x_1, \hat{x}_1$ and $x_2, \hat{x}_2$ by varying irradiation condition. Figure 7a, b shows the estimation errors $\tilde{x}_1$ and $\tilde{x}_2$. Estimation error is almost zero except at interval at 0.5 s.

5.7 Robustness to the parasitics

The control of the converter becomes difficult in the presence of parasitics (model uncertainties) and external disturbances. These model uncertainties are introduced by 10% modulation of the converter parameters L, C, R. The new values of L, C and R are 1.5 mH , 517 μF and 110 Ω, respectively. Figure 8 shows the plot for power response under the variation of parasitics and standard condition (without parasitics). Both the plots are exactly coinciding with each other showing that the performance of the controller remains same in the presence of model uncertainties. The power response under variation of parasitics is shown in Fig. 9. The proposed controller is shown by black color, and the response of the controller (Mojallizadeh et al. 2016) is shown by red color. It

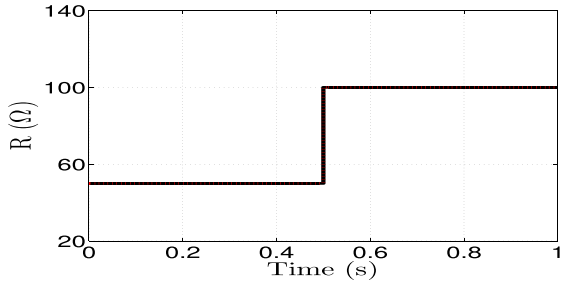

(a) Load Variation

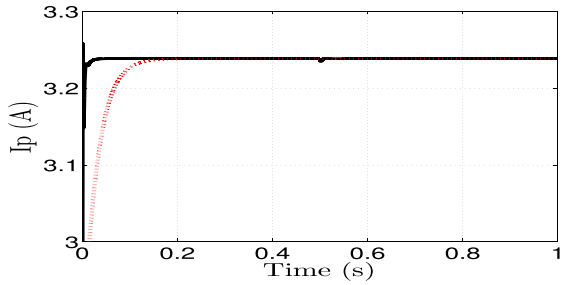

(b) Solar panel output current variation

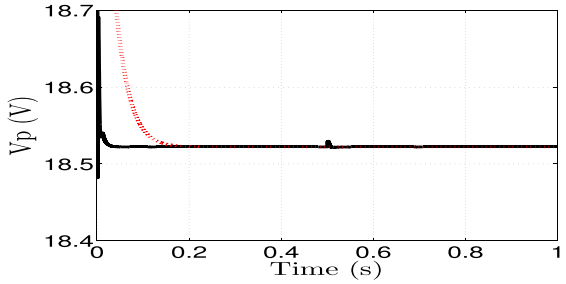

(c) Solar panel output voltage variation

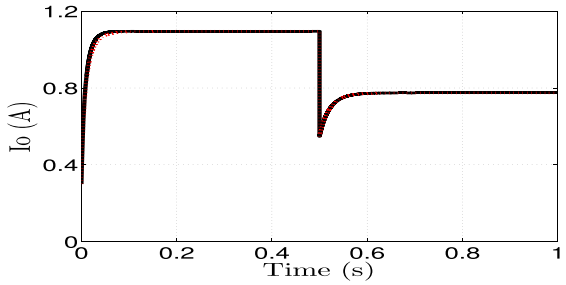

(d) Converter output current variation

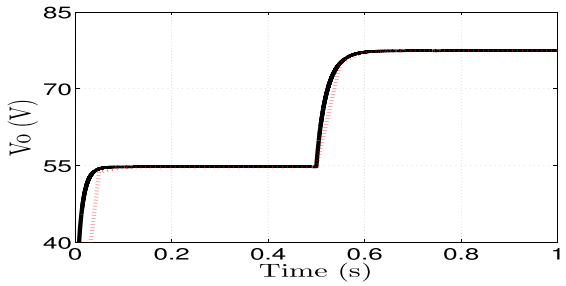

(e) Converter output voltage variation

Fig. 4 Comparison of the proposed method (black) with (Mojallizadeh et al. 2016) (dotted red) under varying load condition (Case 3) (Color figure online)

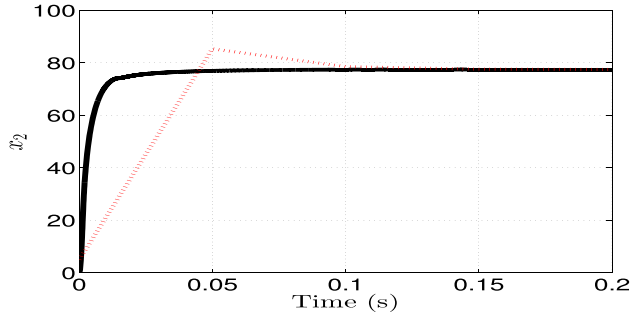

(a) Output voltage

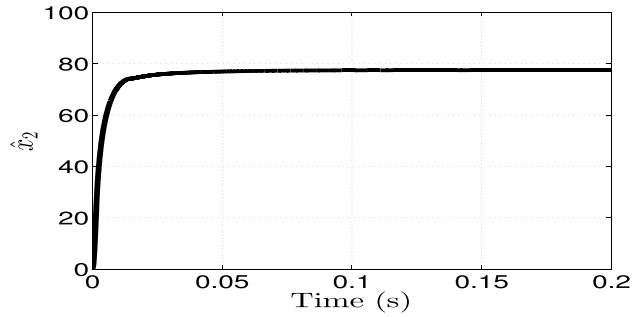

(b) Estimate of output voltage

Fig. 5 Response for the initial condition proposed (black) and Mojallizadeh et al. (2016) (dotted red) (Color figure online)

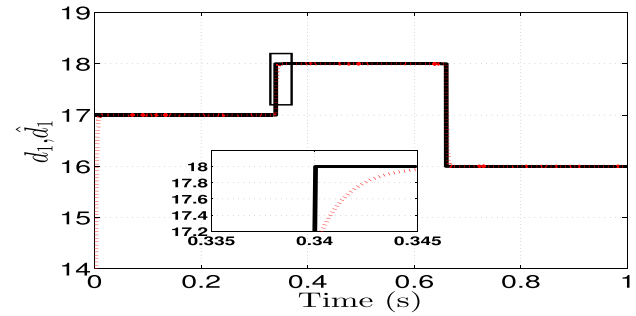

(a)

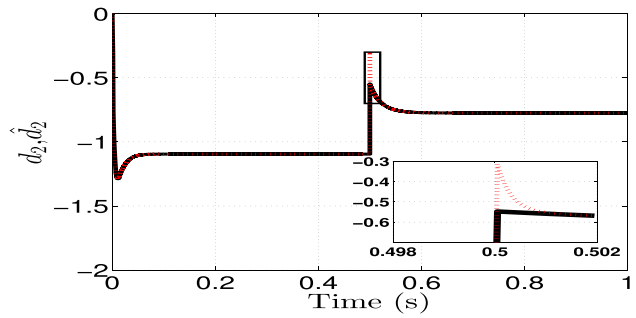

(b)

Fig. 6 Response for **a** d_1 (black) and $\hat{d}_1$ (dotted red), **b** d_2(black) and $\hat{d}_2$ (dotted red) (Color figure online)

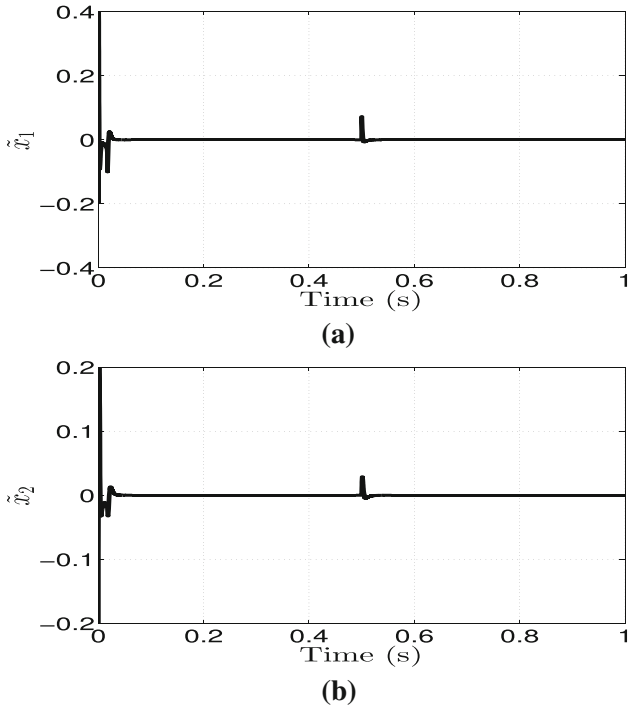

Fig. 7 Response for **a** Estimation error $\tilde{x}_1$, **b** estimation error $\tilde{x}_2$

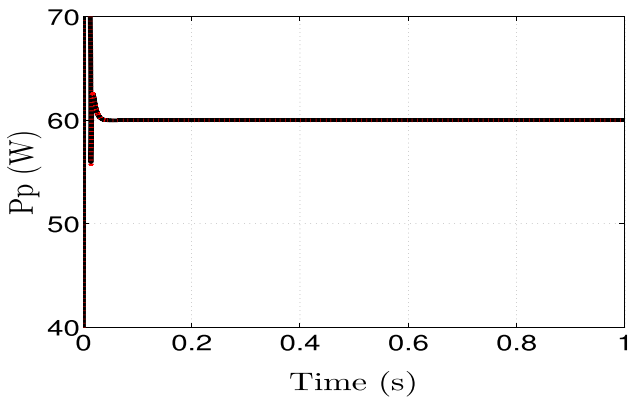

Fig. 8 Power response for the proposed with parasitics (black) and at standard condition without parasitics (dotted red) (Color figure online)

is observed that the proposed controller works satisfactorily in spite of modulation of the converter parameter.

6 Experimentation results

In this section, the scheme is validated by experimentation. The experimental setup is shown in Fig. 10. The setup consists of programmable power supply which mimics a solar simulator, a dc–dc converter, current sensor assembly and Dspace 1104 module. The control algorithm generates control input u which is fed to the converter in the form of PWM signal. The switching frequency is kept constant at 100 kHz.

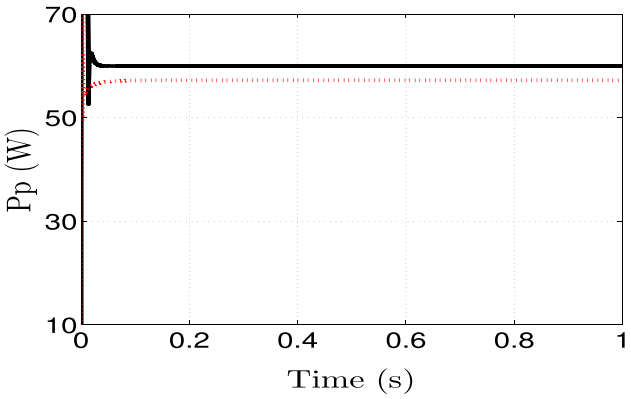

Fig. 9 Power response for the proposed (black) and Mojallizadeh et al. (2016) (dotted red) (Color figure online)

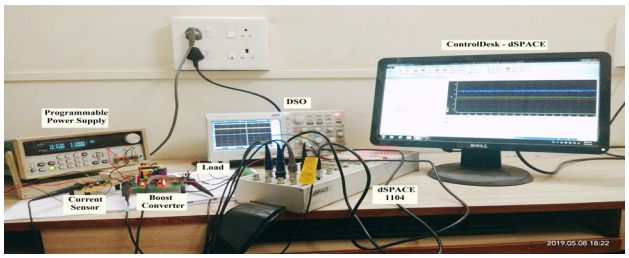

Fig. 10 Experimental setup

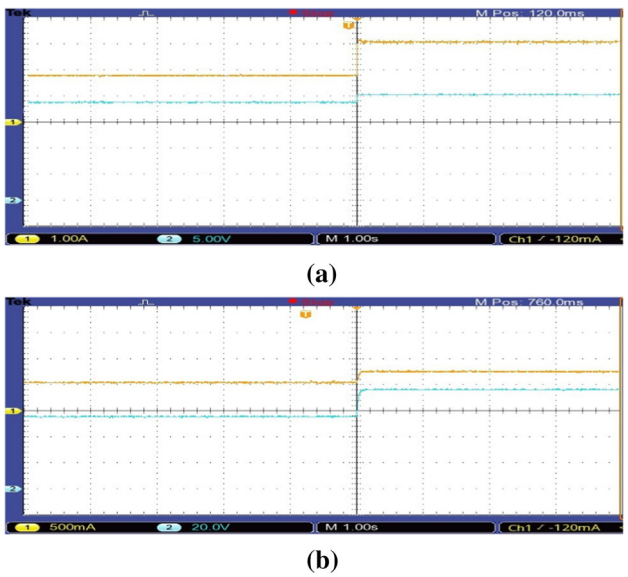

Fig. 11 Response for 550–1000 W/m^2 irradiation change **a** I_{pv} (yellow: 1 A/div), V_{pv} (blue: 5 V/div), **b** I_o (yellow: 500 mA/div), V_o (blue: 20 V/div) (Color figure online)

Figure 11a, b gives the variation of solar panel output current and voltage, converter output current and voltage experimentation graphs for variation of the irradiation. The irradiation is varied from 550 to 1000 W/m^2. The I_{pv} and V_{pv} vary from 1.7 to 3.2 A and 17.8–15.5 V, respectively. The I_o and V_o vary from 0.56 to 0.77 A and 56 to 77 V, respectively. The

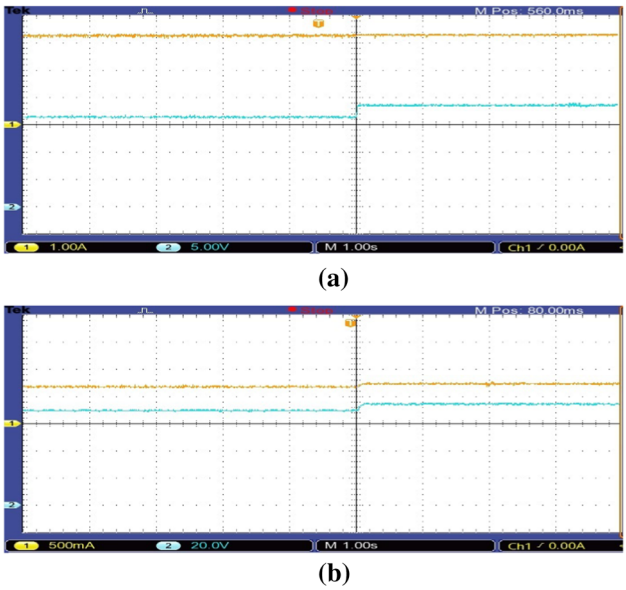

Fig. 12 Response for 50–25 °C temperature change **a** I_{pv} (yellow: 1 A/div), V_{pv} (blue: 5 V/div), **b** I_o (yellow: 500 mA/div), V_o (blue: 20 V/div) (Color figure online)

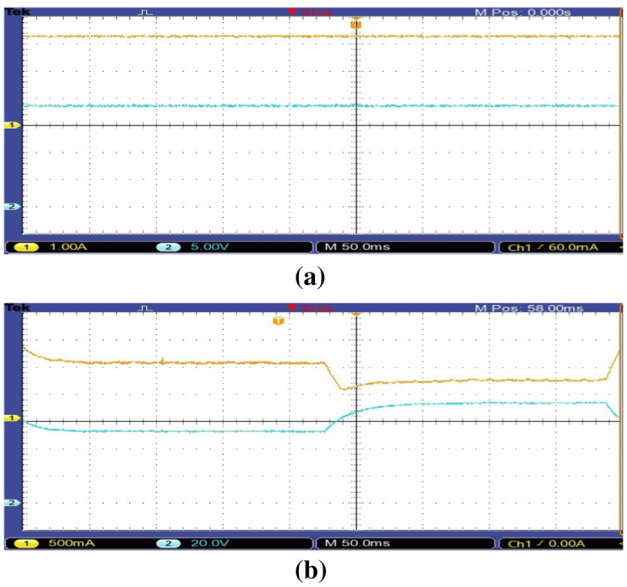

Fig. 13 Response for 50–100 Ω load change **a** I_{pv} (yellow: 1 A/div), V_{pv} (blue: 5 V/div), **b** I_o (yellow: 500 mA/div), V_o (blue: 20 V/div) (Color figure online)

algorithm retains the value of the power constant in the presence of change in the load condition if a change in load is in within the appropriate limit. Figure 12a, b gives the variation of solar panel output current and voltage, converter output current and voltage experimentation graphs for the variation of the temperature. The temperature is varied from 50 to 25 °C. The I_p and V_p vary from 3.29 to 3.23 A and 16.41 to 18.52 V, respectively. The I_o and V_o vary from 0.73 to 0.77 A and 72 to 77 V, respectively. A decrease in temperature gives an increase in the power value and vice versa. Figure 13a, b gives the variation of solar panel output current and voltage, converter output current and voltage experimentation graphs for the variation of the load. The load resistance is varied from 50 to 100 Ω. The I_{pv} and V_{pv} vary from 3.2 to 3.2 A and 18.52 to 18.52 V, respectively. The I_o and V_o vary from 1.1 to 0.7 A and 54.7–77.1 V, respectively. A decrease in temperature gives an increase in the power value. The simulation and experiment are carried out for all possible combinations of the environmental change, and results are obtained. The proposed algorithm tracks the maximum power effectively. Simulation and experimentation result analysis proves the robustness of the proposed algorithm.

7 Conclusion

A new observer-based control is proposed, analyzed and validated in this work. The proposed controller is validated for uncertain load variation and environmental conditions. The combination of DO with SMC successfully robustified the system against uncertain load with chatter-free control and saved the use of a sensor to measure V_p which is marked improvement over many existing results. The novel state observer and the sliding surface based on an estimate of a solar panel output current enabled operating the system from zero initial value of converter output voltage.

References

Abdel-Salam, M., El-Mohandes, M.-T., & Goda, M. (2018). An improved perturb-and-observe based MPPT method for PV systems under varying irradiation levels. *Solar Energy*, *171*, 547–561.

Abolvafaei, M., & Ganjefar, S. (2019). Maximum power extraction from a wind turbine using second-order fast terminal sliding mode control. *Renewable Energy*, *139*, 1437–1446.

Alajmi, B. N., Ahmed, K. H., Finney, S. J., & Williams, B. W. (2011). Fuzzy-logic-control approach of a modified hill-climbing method for maximum power point in microgrid standalone photovoltaic system. *IEEE Transactions on Power Electronics*, *26*(4), 1022–1030.

Alghuwainem, S. (1994). Matching of a dc motor to a photovoltaic generator using a step-up converter with a current-locked loop. *IEEE Transactions on Energy Conversion*, *9*(1), 192–198.

Chen, M., Shao, S.-Y., Shi, P., & Shi, Y. (2017). Disturbance-observer-based robust synchronization control for a class of fractional-order chaotic systems. *IEEE Transactions on Circuits and Systems II*, *64*(4), 417–421.

Chen, W.-H. (2004). Disturbance observer based control for nonlinear systems. *IEEE/ASME Transactions on Mechatronics*, *9*(4), 706–710.

Chen, W.-H., Yang, J., Guo, L., & Li, S. (2016). Disturbance-observer-based control and related methods|an overview. *IEEE Transactions on Industrial Electronics*, *63*(2), 1083–1095.

Chu, C.-C., & Chen, C.-L. (2009). Robust maximum power point tracking method for photovoltaic cells: A sliding mode control approach. *Solar Energy*, *83*(8), 1370–1378.

Corless, M., & Leitmann, G. (1981). Continuous state feedback guaranteeing uniform ultimate boundedness for uncertain dynamic systems. *IEEE Transactions on Automatic Control*, *26*(5), 1139–1144.

Dhar, S., & Dash, P. (2015). A finite time fast terminal sliding mode i–v control of grid-connected pv array. *Journal of Control, Automation and Electrical Systems*, *26*(3), 314–335.

Esram, T., Kimball, J. W., Krein, P. T., Chapman, P. L., & Midya, P. (2006). Dynamic maximum power point tracking of photovoltaic arrays using ripple correlation control. *IEEE Transactions on Power Electronics*, *21*(5), 1282–1291.

Femia, N., Petrone, G., Spagnuolo, G., & Vitelli, M. (2005). Optimization of perturb and observe maximum power point tracking method. *IEEE Transactions on Power Electronics*, *20*(4), 963–973.

Ginoya, D., Shendge, P., & Phadke, S. (2014). Sliding mode control for mismatched uncertain systems using an extended disturbance observer. *IEEE Transactions on Industrial Electronics*, *61*(4), 1983–1992.

Glasner, I., & Appelbaum, J. (1996). Advantage of boost versus buck topology for maximum power point tracker in photovoltaic systems. In *Nineteenth convention of Electrical and electronics engineers in Israel, 1996* (pp. 355–358).

Heydari-doostabad, H., Keypour, R., Khalghani, M. R., & Khooban, M. H. (2013). A new approach in mppt for photovoltaic array based on extremum seeking control under uniform and non-uniform irradiances. *Solar Energy*, *94*, 28–36.

Lin, C.-H., Huang, C.-H., Du, Y.-C., & Chen, J.-L. (2011). Maximum photovoltaic power tracking for the pv array using the fractional-order incremental conductance method. *Applied Energy*, *88*(12), 4840–4847.

Moçambique, N. E., Ottoboni, K. D. A., Fuzato, G. H., Bastos, R. F., Gonçalves, A. F., Pozzebon, G. G., et al. (2015). Tracking algorithms and voltage controllers used to obtain the maximum power point of pv arrays. *Journal of Control, Automation and Electrical Systems*, *26*(6), 661–674.

Mojallizadeh, M. R., Badamchizadeh, M., Khanmohammadi, S., & Sabahi, M. (2016). Designing a new robust sliding mode controller for maximum power point tracking of photovoltaic cells. *Solar Energy*, *132*, 538–546.

Rezaei, M. A. (2019). A modified perturb-and-observe-based maximum power point tracking technique for photovoltaic energy conversion systems. *Journal of Control, Automation and Electrical Systems*, *30*, 822–831.

Salas, V., Olias, E., Barrado, A., & Lazaro, A. (2006). Review of the maximum power point tracking algorithms for stand-alone photovoltaic systems. *Solar Energy Materials and Solar Cells*, *90*(11), 1555–1578.

Sitbon, M., Schacham, S., & Kuperman, A. (2015). Disturbance observer-based voltage regulation of current-mode-boost-converter-interfaced photovoltaic generator. *IEEE Transactions on Industrial Electronics*, *62*(9), 5776–5785.

Subudhi, B., & Pradhan, R. (2013). A comparative study on maximum power point tracking techniques for photovoltaic power systems. *IEEE Transactions on Sustainable Energy*, *4*(1), 89–98.

Utkin, V. I. (1993). Sliding mode control design principles and applications to electric drives. *IEEE Transactions on Industrial Electronics*, *40*(1), 23–36.

Veerachary, M., Senjyu, T., & Uezato, K. (2003). Neural-network-based maximum-power-point tracking of coupled-inductor interleaved-boost-converter supplied pv system using fuzzy controller. *IEEE Transactions on Industrial Electronics*, *50*(4), 749–758.

Yong, Y., & Huiqing, W. (2019). Adaptive perturb and observe maximum power point tracking with current predictive and decoupled power control for grid connected photovoltaic inverters. *Journal of Modern Power Systems and Clean Energy*, *7*(2), 422–432.

Zhang, J., Liu, X., Xia, Y., Zuo, Z., & Wang, Y. (2016). Disturbance observer-based integral slidingmode control for systems with mismatched disturbances. *IEEE Transactions on Industrial Electronics*, *63*(11), 7040–7048.